

Charge dynamics in strongly-correlated electronic systems

Nguyen Dan Tung

Institute of Physics,

*Viet Nam Academy of Science and Technology,
10 Dao Tan, Ba Dinh, Hanoi 1000, Viet Nam*

*Joint Institute for Nuclear Research, Dubna 141980, Russia
nguen@theor.jinr.ru*

Nikolay Plakida*

*Joint Institute for Nuclear Research, Dubna 141980, Russia
plakida@theor.jinr.ru*

Received 15 July 2018

Revised 21 September 2018

Accepted 2 October 2018

Published 14 November 2018

We consider the dynamic charge susceptibility and the charge density waves in strongly-correlated electronic systems within the two-dimensional t - J - V model. Using the equation of motion method for the relaxation functions in terms of the Hubbard operators, we calculate the static susceptibility and the spectrum of charge fluctuations as functions of doped hole concentrations and temperature. Charge density waves emerge for a sufficiently strong intersite Coulomb interaction. Calculation of the dynamic charge susceptibility reveals a strong damping of charge density waves for a small hole doping and propagating high-energy charge excitations at large doping.

Keywords: Strong electron correlation; dynamic charge susceptibility; t - J - V model.

PACS numbers: 71.10.-w, 71.27.+a, 71.45.Lr

1. Introduction

Among other unconventional normal state properties of high- T_c superconductors (see, e.g., Ref. 1), an anomalous charge dynamics and charge-density wave (CDW) formation have been also recently detected. Using optical methods and the resonance inelastic X-ray scattering, this phenomenon was observed in many experiments on copper oxide compounds. The CDWs were found in the compounds YBCO (see Refs. 2–5 and references therein), Bi-2201,⁶ Bi-2212^{7–10} and Hg-1201.^{11,12}

*Corresponding author.

In all compounds, CDWs have similar characteristics: they arise in the CuO_2 plane in the underdoped region at temperatures T_{CDW} below or nearly equal to the temperature of the pseudo-gap state T^* but above the temperature of the superconducting transition T_c . They are characterized by the incommensurable wave-vector $(q_x, q_y) = 0.2\text{--}0.3$ (in units of the reciprocal lattice vector) and have a short correlation length of about 5–8 lattice constants. Charge modulation occurs at the sites of the oxygen sublattice and has d -symmetry. In particular, in YBCO compound in Ref. 2 CDW was found at hole doping $0.086 < p < 0.163$ at the incommensurable wave-vector in the direction $(1,0,0)$ ($0.34 \lesssim q_x \lesssim 0.30$) which is decreasing with doping in the temperature range $T = 100 - 160$ K. In Bi2201 compound in Ref. 10 CDW was found at hole doping $0.07 \lesssim p \lesssim 0.16$ at the incommensurable wave-vector in the direction $(1,0,0)$ ($0.23 \lesssim q_x \lesssim 0.26$) which is decreasing with doping in the temperature range $T = 20\text{--}125$ K for an optimally doped sample with $T_c = 33$ K and the pseudogap temperature $T^* = 160$ K.

In the theoretical description of CDWs in cuprates in several papers, the Fermi-liquid approximation was used. In Ref. 13, an interplay between unidirectional and bidirectional CDW orders in underdoped cuprates was considered within a phenomenological theory. A magnetic scenario has been proposed when CDW order appears due to spin-fluctuation exchange where a bidirectional CDW order emerges at the onset but changes to unidirectional inside the CDW phase. In Ref. 14, an interplay between the CDW instability and the pseudogap phase was considered within the random-phase approximation (RPA) for correlated singleband quasi-particles described by a Fermi-liquid type model. A microscopical theory of the electron-hole instability due to the development of CDW at the oxygen sites in the copper oxide plane was formulated within the spin-fermion model in Ref. 15 (for further references within the Fermi-liquid approach, see Ref. 15).

However, cuprates are strongly correlated systems and the Fermi-liquid description cannot be applied. In that case, the Hubbard model¹⁶ is often considered where numerical methods, such as the quantum Monte Carlo (QMC) method, were used in analyzing CDWs (see, e.g., Ref. 17). Charge fluctuations within the original t - J model were considered by QMC in Ref. 18. In the limit of strong correlations, the Hubbard model can be reduced to the t - J model with the intersite Coulomb repulsion V , the so-called t - J - V model, which is suitable for CDW description. In particular, in the framework of this model, development of CDW and formation of the pseudogap in the normal state of cuprates were considered in Refs. 19–21. The correlation of CDWs with the softening of the longitudinal phonon mode in cuprates was analyzed in Ref. 22. In these papers, the random-phase-type approximation was considered when the density operator on one lattice site is presented as an electron-hole pair similar to the Fermi-liquid approach. However, this approximation is difficult to justify in the case of strong correlations described by the Hubbard operators.¹⁶

An accurate method is based on the projection technique for the time-dependent correlation functions²³ or the Green functions (GFs).^{24,25} Using this approach, we

can obtain an exact representation for the GF for the charge or spin collective excitations with the polarization operator, which is then calculated self-consistently in terms of the full GF. Within this method, we have considered the spectra of antiferromagnetic spin excitations for the high-temperature superconductors in the framework of the t - J model in both the normal,²⁶ and superconducting²⁷ phases and also the optical conductivity.²⁸ Here, we calculate the dynamical charge susceptibility (DCS) in the framework of the t - J - V model in terms of the Hubbard operators (HOs) using the method of the relaxation function.^{29–31} This approach was previously used in the framework of the standard t - J model in Ref. 32. The static charge susceptibility was considered for holes in the t - J - V model in our previous publication.³³ In the present paper, we calculate the DCS for the electronic t - J - V model by taking into account final life-time effects. We also calculate the spectrum of electronic excitations for the t - J - V model using the projection method for the single-particle GF similar to Ref. 34 for the t - J model.

In Sec. 2, we formulate the model and calculate the dynamical and static charge susceptibilities. In Sec. 3, we present the results. At first we consider the static charge susceptibility (Sec. 3.1) analyzing conditions for providing the CDWs and then we describe the spectrum of charge fluctuations by taking into account their damping (Sec. 3.2). The results are presented in Sec. 4. In Appendix, details of the calculations are discussed.

2. The Model and the Dynamical Charge Susceptibility

2.1. The t - J - V model

To describe strongly-correlated electronic systems, we consider the t - J - V model where in addition to the conventional hopping t and exchange interaction J terms, the intersite Coulomb repulsion V is taken into account. It is convenient to use the HO technique^{16,35} and to write the model as follows (see, e.g., Ref. 34):

$$\begin{aligned}
 H = H_t + H_J + H_c = & - \sum_{i \neq j, \sigma} t_{ij} X_i^{\sigma 0} X_j^{0 \sigma} - \mu \sum_{i \sigma} X_i^{\sigma \sigma} \\
 & + \frac{1}{4} \sum_{i \neq j, \sigma} J_{ij} (X_i^{\sigma \bar{\sigma}} X_j^{\bar{\sigma} \sigma} - X_i^{\sigma \sigma} X_j^{\bar{\sigma} \bar{\sigma}}) + \frac{1}{2} \sum_{i \neq j} V_{i,j} N_i N_j, \quad (1)
 \end{aligned}$$

where the HOs $X_i^{\alpha\beta} = |i\alpha\rangle\langle i\beta|$ describe transitions from the state $|i, \beta\rangle$ to the state $|i, \alpha\rangle$ on the lattice site i for the three electronic states with spin $\sigma/2$, $\sigma = \pm 1$ ($\bar{\sigma} = -\sigma$): the unoccupied state ($\alpha, \beta = 0$) and two singly occupied states ($\alpha, \beta = \sigma$). The projected electron operators commonly used in description of electrons in the singly occupied subband in the t - J model represented by $\tilde{a}_{i,\sigma}^\dagger = a_{i,\sigma}^\dagger(1 - n_{i,\bar{\sigma}})$ and $\tilde{a}_{i,\sigma} = a_{i,\sigma}(1 - n_{i,\bar{\sigma}})$ in terms of the original creation and annihilation Fermi operators $a_{i,\sigma}^\dagger, a_{i,\sigma}$ can be written as the HOs $X_i^{\sigma 0} = \tilde{a}_{i,\sigma}^\dagger$ and $X_i^{0 \sigma} = \tilde{a}_{i,\sigma}$.

In (1), we introduce the hopping parameters $t_{ij} = t\delta_{j,i+\mathbf{a}_1} + t'\delta_{j,i+\mathbf{a}_2} + t''\delta_{j,i+\mathbf{a}_3}$ between the first t ($\mathbf{a}_1 = \pm a_x, \pm a_y$), the second t' ($\mathbf{a}_2 = \pm(a_x \pm a_y)$), and the third

t'' ($\mathbf{a}_3 = \pm 2a_x, \pm 2a_y$) neighbors, respectively, ($a_x = a_y$ - are the two-dimensional lattice constants). $J_{ij} = J\delta_{j,i+\mathbf{a}_1}$ is the exchange interaction for the nearest neighbors. The intersite Coulomb interaction (CI) $V_{ij} = V_1\delta_{j,i+\mathbf{a}_1} + V_2\delta_{j,i+\mathbf{a}_2}$, where V_1 and the V_2 are CI between the first and the second neighbors, respectively. The Fourier components of the hopping parameter $t(\mathbf{q})$, CI $V(\mathbf{q})$ and the exchange interaction $J(\mathbf{q})$ on the square lattice are given by

$$t(\mathbf{q}) = 4t\gamma(\mathbf{q}) + 4t'\gamma'(\mathbf{q}) + 4t''\gamma''(\mathbf{q}), \quad (2)$$

$$V(\mathbf{q}) = 4V_1\gamma(\mathbf{q}) + 4V_2\gamma'(\mathbf{q}), \quad (3)$$

$$J(\mathbf{q}) = 4J\gamma(\mathbf{q}), \quad (4)$$

where $\gamma(\mathbf{q}) = (1/2)(\cos q_x + \cos q_y)$, $\gamma'(\mathbf{q}) = \cos q_x \cos q_y$, $\gamma''(\mathbf{q}) = (1/2)(\cos 2q_x + \cos 2q_y)$ and we take $a_x = a_y = a = 1$.

The number and spin operators in HO representation read

$$N_i = \sum_{\sigma} X_i^{\sigma\sigma}, \quad (5)$$

$$S_i^{\sigma} = X_i^{\sigma\bar{\sigma}}, \quad S_i^z = (\sigma/2)(X_i^{\sigma\sigma} - X_i^{\bar{\sigma}\bar{\sigma}}). \quad (6)$$

The chemical potential μ in (1) is determined from the equation for the average number of electrons n as

$$n = \langle N_i \rangle, \quad (7)$$

where $\langle \dots \rangle$ is the statistical average with the Hamiltonian (1).

The HOs satisfy the completeness relation

$$X_i^{00} + X_i^{\sigma\sigma} + X_i^{\bar{\sigma}\bar{\sigma}} = 1, \quad (8)$$

which rigorously preserves the constraint of no double occupancy of any quantum state $|i, \alpha\rangle$ on each lattice site i . From the multiplication rules for HOs $X_i^{\alpha\beta} X_i^{\gamma\delta} = \delta_{\beta\gamma} X_i^{\alpha\delta}$ follow the commutation relations

$$[X_i^{\alpha\beta} X_j^{\gamma\delta}]_{\pm} = \delta_{ij}(\delta_{\beta\gamma} X_i^{\alpha\delta} \pm \delta_{\delta\alpha} X_i^{\gamma\beta}), \quad (9)$$

where the upper sign refers to Fermi-type operators such as $X_i^{0\sigma}$, while the lower sign refers to Bose-type operators such as the number (5) or the spin (6) operators.

2.2. Memory function formalism

To study the dynamic charge fluctuations, we consider the two-time retarded Green function (GF)²⁵

$$G_{\mathbf{q}}(t - t') = \langle\langle N_{\mathbf{q}}(t) | N_{-\mathbf{q}}(t') \rangle\rangle = -i\vartheta(t - t') \langle [N_{\mathbf{q}}(t), N_{-\mathbf{q}}(t')] \rangle, \quad (10)$$

$$N_{\mathbf{q}} = \frac{1}{\sqrt{N}} \sum_i N_i \exp(-i\mathbf{q}\mathbf{r}_i), \quad (11)$$

where $[A, B] = AB - BA$, $N_{\mathbf{q}}(t) = e^{iHt} N_{\mathbf{q}} e^{-iHt}$ (we take $\hbar = 1$) and $\vartheta(t - t')$ is the Heaviside function. The dynamic charge susceptibility (DCS) $\chi_{\mathbf{q}}(\omega)$ is given by

the Fourier transform of the GF (10) as

$$\chi_{\mathbf{q}}(\omega) = -\langle\langle N_{\mathbf{q}} | N_{-\mathbf{q}} \rangle\rangle_{\omega} = i \int_0^{\infty} dt e^{i\omega t} \langle [N_{\mathbf{q}}(t), N_{-\mathbf{q}}] \rangle. \quad (12)$$

A conventional calculation of the GF (10) by differentiating it over time t and a decoupling of the higher-order GFs²⁵ is not convenient for the GF of collective variables as the charge density fluctuations (11). The inhomogeneous term in the GF equation in this case is zero, $[N_{\mathbf{q}}, N_{-\mathbf{q}}] = 0$, that makes it difficult to solve equations. For collective variables, it is more convenient to use the relaxation function approach employing the memory function formalism.^{23,24,29–31} This approach was used in our previous publications.^{32,33}

For this, we introduce the density–density relaxation function

$$\Phi_{\mathbf{q}}(t - t') = ((N_{\mathbf{q}}(t) | N_{-\mathbf{q}}(t'))) = -i\vartheta(t - t')(N_{\mathbf{q}}(t), N_{-\mathbf{q}}(t')), \quad (13)$$

where

$$(A(t), B) = \int_0^{1/T} d\lambda \langle A(t - i\lambda) B \rangle, \quad (14)$$

is the Kubo–Mori scalar product (T is the temperature in units of $k_B = 1$). The Fourier transform of the density–density relaxation function

$$\Phi_{\mathbf{q}}(\omega) = ((N_{\mathbf{q}} | N_{-\mathbf{q}}))_{\omega} = -i \int_0^{\infty} dt e^{i\omega t} (N_{\mathbf{q}}(t), N_{-\mathbf{q}}), \quad (15)$$

is coupled to the GF by the equation $((i\dot{A} | B))_{\omega} = \langle\langle A | B \rangle\rangle_{\omega}$, $i\dot{A} = idA/dt = [A, H]$, that results in the relation

$$\chi_{\mathbf{q}}(\omega) = \chi_{\mathbf{q}} - \omega \Phi_{\mathbf{q}}(\omega), \quad (16)$$

where $\chi_{\mathbf{q}} = \chi_{\mathbf{q}}(0) = (N_{\mathbf{q}}, N_{-\mathbf{q}})$ is the static susceptibility.

Using equations of motion for the time-dependent relaxation function (13), we can write the relaxation function (15) in the form (see Appendix A)

$$\Phi_{\mathbf{q}}(\omega) = \chi_{\mathbf{q}} \frac{\omega - \omega M_{\mathbf{q}}(\omega)/m_{\mathbf{q}}}{\omega^2 - \Omega_{\mathbf{q}}^2 - \omega M_{\mathbf{q}}(\omega)/m_{\mathbf{q}}}, \quad (17)$$

where

$$m_{\mathbf{q}} = (i\dot{N}_{\mathbf{q}} | -i\dot{N}_{-\mathbf{q}}), \quad (18)$$

and $\Omega_{\mathbf{q}}^2 = m_{\mathbf{q}}/\chi_{\mathbf{q}}$ is the energy of density fluctuations in the MFA. The memory function $M_{\mathbf{q}}(\omega)$ is given by the irreducible part of the force–force relaxation function

$$M_{\mathbf{q}}(\omega) = ((F_{\mathbf{q}} | F_{-\mathbf{q}}))_{\omega}^{\text{irr}}. \quad (19)$$

where the force $F_{\mathbf{q}} = \ddot{N}_{\mathbf{q}} = -[[N_{\mathbf{q}}, H], H]$. The irreducible part in Eq. (19) has no parts connected by the corresponding zero-order relaxation function (see Appendix A). This definition is equivalent to the introduction of the projected Liouville operator for time dependence of correlation functions in the Mori method.²³

Using Eq. (16) for the DCS (12), we obtain the following representation:

$$\chi_{\mathbf{q}}(\omega) = \chi_{\mathbf{q}} - \omega\Phi_{\mathbf{q}}(\omega) = \frac{m_{\mathbf{q}}}{\Omega_{\mathbf{q}}^2 + \omega M_{\mathbf{q}}(\omega)/m_{\mathbf{q}} - \omega^2}. \quad (20)$$

The spectral density of charge fluctuations is determined by the imaginary part of the DCS

$$I_{\mathbf{q}}(\omega) = \text{Im}\chi_{\mathbf{q}}(\omega + i\varepsilon) = \frac{m_{\mathbf{q}} 2\omega\Gamma_{\mathbf{q}}(\omega)}{[\Omega_{\mathbf{q}}^2 + 2\omega\Delta_{\mathbf{q}}(\omega) - \omega^2]^2 + [2\omega\Gamma_{\mathbf{q}}(\omega)]^2}, \quad (21)$$

where we introduce the imaginary and real parts of the memory function

$$\Gamma_{\mathbf{q}}(\omega) = -(1/2 m_{\mathbf{q}})\text{Im}M_{\mathbf{q}}(\omega + i\varepsilon), \quad \Delta_{\mathbf{q}}(\omega) = (1/2 m_{\mathbf{q}})\text{Re}M_{\mathbf{q}}(\omega + i\varepsilon). \quad (22)$$

To calculate the energy of density fluctuations $\Omega_{\mathbf{q}}$ and the static susceptibility $\chi_{\mathbf{q}} = m_{\mathbf{q}}/\Omega_{\mathbf{q}}^2$, we consider the relation

$$m_{\mathbf{q}} = (i\dot{N}_{\mathbf{q}} | -i\dot{N}_{-\mathbf{q}}) = (-\ddot{N}_{\mathbf{q}}, N_{-\mathbf{q}}) \approx \Omega_{\mathbf{q}}^2 (N_{\mathbf{q}}, N_{-\mathbf{q}}), \quad (23)$$

where the left-hand side is found directly using the commutation relations for the HOs (see Appendix A)

$$m_{\mathbf{q}} = \langle [i\dot{N}_{\mathbf{q}}, N_{-\mathbf{q}}] \rangle = \frac{4}{N} \sum_{\mathbf{q}'} [t(\mathbf{q}') - t(\mathbf{q} - \mathbf{q}')] \langle X_{\mathbf{q}'}^{\sigma 0} X_{\mathbf{q}'}^{0\sigma} \rangle. \quad (24)$$

For the right-hand side of Eq. (23), the higher-order correlation functions in $(-\ddot{N}_{\mathbf{q}}, N_{-\mathbf{q}}) = ([N_{\mathbf{q}}, H], H, N_{-\mathbf{q}})$ are calculated in the MFA approximation (see Appendix A). As a result, the charge excitation energy takes the form

$$\begin{aligned} \Omega_{\mathbf{q}}^2 &= \frac{(-\ddot{N}_{\mathbf{q}}, N_{-\mathbf{q}})}{(N_{\mathbf{q}}, N_{-\mathbf{q}})} = \frac{1}{N} \sum_{\mathbf{q}'} [t(\mathbf{q}') - t(\mathbf{q} - \mathbf{q}')] \\ &\times \left(t(\mathbf{q}') - \frac{1}{2}J(\mathbf{q}) + 2V(\mathbf{q}) \right) \langle X_{\mathbf{q}'}^{\sigma 0} X_{\mathbf{q}'}^{0\sigma} \rangle + \text{H.c.} \end{aligned} \quad (25)$$

We note that for the short-range CI considered here, the charge excitation spectrum is characterized by the acoustic mode $\Omega_{\mathbf{q}} \propto q$ and the uniform static charge susceptibility $\chi_{\mathbf{q} \rightarrow \mathbf{0}} = (m_{\mathbf{q}}/\Omega_{\mathbf{q}}^2)_{\mathbf{q} \rightarrow \mathbf{0}}$ is finite.

The charge fluctuation correlation function $\langle N_{\mathbf{q}} N_{-\mathbf{q}} \rangle$ in the MFA for the DCS (20) (for $M_{\mathbf{q}}(\omega) = 0$) is given by

$$\langle N_{\mathbf{q}} N_{-\mathbf{q}} \rangle = \int_{-\infty}^{\infty} \frac{d\omega}{\exp(\omega/T) - 1} \frac{1}{\pi} \text{Im}\chi(\mathbf{q}, \omega + i\varepsilon) = \frac{m_{\mathbf{q}}}{2\Omega_{\mathbf{q}}} \coth \frac{\Omega_{\mathbf{q}}}{2T}. \quad (26)$$

We assume that using the MFA for DCS instead of the full representation (20) does not change noticeably results for the thermodynamical functions as (26). In particular, in the classical limit, $\Omega_{\mathbf{q}} \ll T$, we obtain the conventional relation between the correlation function and the charge susceptibility: $\langle N_{\mathbf{q}} N_{-\mathbf{q}} \rangle = T\chi_{\mathbf{q}}$. In the quantum limit for $T = 0$, we have $\langle N_{\mathbf{q}} N_{-\mathbf{q}} \rangle = m_{\mathbf{q}}/2\Omega_{\mathbf{q}}$ and $[m_{\mathbf{q}}/2\Omega_{\mathbf{q}}]_{q \rightarrow 0} = 0$.

To calculate the electronic correlation function $\langle X_{\mathbf{q}}^{\sigma 0} X_{\mathbf{q}}^{0\sigma} \rangle$ in Eqs. (24) and (25) and the chemical potential in Eq. (7), we use results for the corresponding electronic GF in the generalized MFA (see Appendix B) as

$$\langle X_{\mathbf{q}}^{\sigma 0} X_{\mathbf{q}}^{0\sigma} \rangle = N_{\sigma}(\mathbf{q}) = \frac{1 - n/2}{\exp[\tilde{\varepsilon}(\mathbf{q})/T] + 1}, \quad (27)$$

$$n = \frac{1}{N} \sum_{\mathbf{q}, \sigma} N_{\sigma}(\mathbf{q}) = \frac{1}{N} \sum_{\mathbf{q}} \frac{(2 - n)}{\exp[\tilde{\varepsilon}(\mathbf{q})/T] + 1}, \quad (28)$$

where the renormalized spectrum of electronic excitation $\tilde{\varepsilon}(\mathbf{q})$ is given by Eq. (B.5). As follows from Eq. (28), for the electronic occupation number we have a restriction $n \leq 1$.

3. Results

In numerical computations we use the following parameters in the model (1). To reproduce the realistic electronic spectrum for cuprates which shows a transition with doping from the four-pockets Fermi surface (FS) to a large one (see, e.g., Ref. 1), we take the hopping parameters $t' = 0.1t$, $t'' = 0.2t$. These parameters result in the electronic excitation spectrum and the FS in a form corresponding to the ones obtained in the Hubbard model^{36,37} (see Appendix B). We take conventional values of the parameters for the t - J model for cuprates $t = 0.4$ eV and $J = 0.4t$. In what follows, we take t as the energy unit and put $t = 1$. According to the model calculations,³⁸ the intersite CI in cuprates is sufficiently small and the parameters in (3), can be chosen as $V_1 = 0.3t$ and $V_2 = 0.2t$. To study the formation of the CDWs, we vary these parameters in a certain range.

3.1. Static charge susceptibility

At first, us consider the spectrum of charge excitation energy (25) and the static charge susceptibility $\chi_{\mathbf{q}} = m_{\mathbf{q}}/\Omega_{\mathbf{q}}^2$ for various doping and temperature. The spectrum of the charge excitations $\Omega_{\mathbf{q}}^2$ along the main directions in the BZ $\Gamma(0,0) \rightarrow X(\pi,0) \rightarrow M(\pi,\pi) \rightarrow \Gamma(0,0)$ is shown in Fig. 1 for electron concentrations $n = 0.9$ and $n = 0.7$ with the standard model parameters $V_1 = 0.3$ and $V_2 = 0.2$ in Eq. (3) and the temperature $T = 0.02 \sim 90$ K. At the center of the BZ $\Gamma(0,0)$, the excitation energy tends to zero, $\Omega_{\mathbf{q}}^2 \propto q^2$. At the boundary of the BZ at the point $M(\pi,\pi)$ the maximum is observed, and its intensity increases with electron concentration. The dispersion of the spectrum depends on the model parameters. It weakly depends on the exchange interaction J but shows a strong variation with the CI parameters V_1 and V_2 as discussed below.

The dependence of the static charge susceptibility $\chi_{\mathbf{q}} = m_{\mathbf{q}}/\Omega_{\mathbf{q}}^2$ on the electron concentration shows a complicated character as shown in Fig. 2. When the spectrum $\Omega_{\mathbf{q}}^2$ has the maximum at the point $M(\pi,\pi)$ of the BZ, the static charge susceptibility $\chi_{\mathbf{q}}$ has the minimum and vice versa. We note that the maximum of the static charge susceptibility found in Ref. 21 is near the point $M(\pi,\pi)$. But the

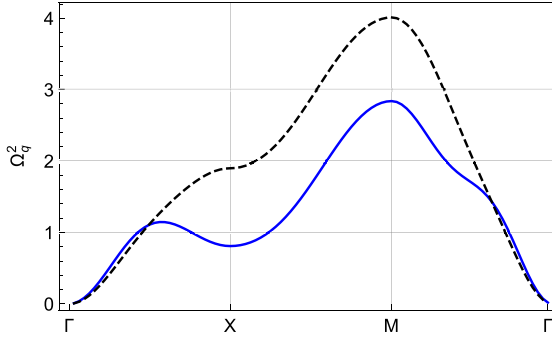


Fig. 1. (Color online) Spectrum of charge excitations Ω_q^2 along the main directions in the BZ: $\Gamma(0,0) \rightarrow X(\pi,0) \rightarrow M(\pi,\pi) \rightarrow \Gamma(0,0)$ for $n = 0.7$ (blue, solid line), $n = 0.9$ (black dash line).

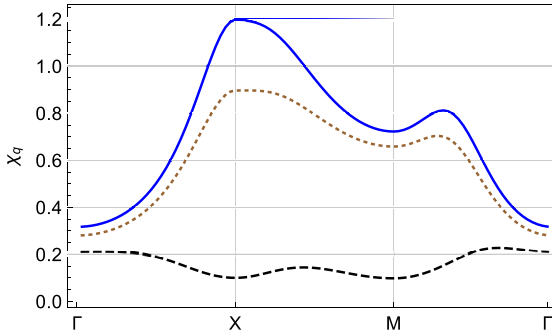


Fig. 2. (Color online) Static charge susceptibility χ_q along the main directions in the BZ: $\Gamma(0,0) \rightarrow X(\pi,0) \rightarrow M(\pi,\pi) \rightarrow \Gamma(0,0)$ for $n = 0.7$ (blue, solid line), $n = 0.8$ (brown, dotted line), $n = 0.9$ (black, dash line).

position of the maximum changes depending on the CI, as shown below. For certain model parameters, the static charge susceptibility diverges which indicates the instability of the uniform charge distribution and formation of the CDW. To analyze this instability, it seems convenient to consider the inverse charge susceptibility $\chi_{\mathbf{q}}^{-1}$ which vanishing indicates a transition to the nonuniform state. Figure 3 shows the dependence of $\chi_{\mathbf{q}}^{-1}$ on the parameter V_1 at a fixed $V_2 = 0.2$. As the parameter V_1 increases, the maximum of the static charge susceptibility (minimum of $\chi_{\mathbf{q}}^{-1}$) shifts from the point $X(\pi,0)$ to the point $M(\pi,\pi)$. At $V_1 \gtrsim 0.6$, the inverse charge susceptibility becomes negative near this point, which indicates instability of the uniform charge distribution and formation of the CDW. As the parameter V_1 increases, the CDW arises near $M(\pi,\pi)$ point of the BZ. The wave-vector of the CDW increases and, e.g., at $V_1 = 0.9$ it equals to $q_x = q_y \approx 0.87(\pi/a)$. A similar strong variation is also observed for $\chi_{\mathbf{q}}^{-1}$ under changes in the parameter V_2 at a fixed $V_1 = 0.3$ as shown in Fig. 4. As the parameter V_2 increases to $V_2 \gtrsim 0.4$, the CDW arises near $X(\pi,0)$ point. At $V_2 = 0.6$, the CDW wave-vector $q_x \approx 0.71(\pi/a)$. Therefore, depending on the CI parameters V_1 and V_2 , which have different symmetries according

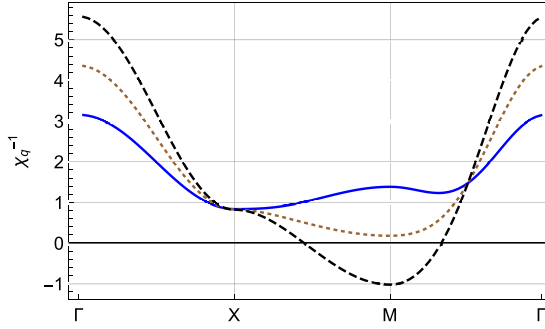


Fig. 3. (Color online) Inverse static charge susceptibility χ_q^{-1} for $n = 0.7$ at $V_2 = 0.2$ depending on the parameter V_1 : $V_1 = 0.3$ (blue, solid line), $V_1 = 0.6$ (brown, dotted line), $V_1 = 0.9$ (black, dash line).

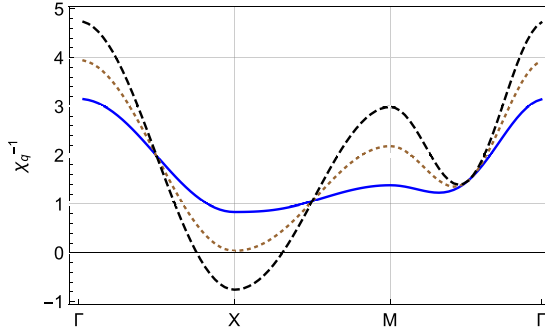


Fig. 4. (Color online) Inverse static charge susceptibility χ_q^{-1} for $n = 0.7$ at $V_1 = 0.3$ depending on the parameter V_2 : $V_2 = 0.2$ (blue, solid line), $V_2 = 0.4$ (brown, dotted line), $V_2 = 0.6$ (black, dash line).

to (3), CDWs can arise either along the direction $\Gamma(0,0) \rightarrow M(\pi,\pi)$ as V_1 increases or along the direction $\Gamma(0,0) \rightarrow X(\pi,0)$ as V_2 increases. As mentioned above, the static charge susceptibility is finite as $q \rightarrow 0$ and shows no instability. As discussed in Sec. 1, in experiments CDWs were found in the quasi-elastic energy region at small wave-vectors $q_x = 0.2 - 0.3$, which we also observed for the dynamical charge susceptibility at low-energy as discussed in the next section.

The charge fluctuation correlation function $\langle N_q N_{-q} \rangle$ (26) depending on the electronic concentration is shown in Fig. 5. Its doping and the wave-vector dependence resembles the one of the static susceptibility χ_q . In the classical limit, at high-temperatures $\langle N_q N_{-q} \rangle = T \chi_q$. The temperature dependence of the static charge susceptibility χ_q and $\langle N_q N_{-q} \rangle$ is weak because of the weak temperature dependence of the functions m_q and Ω_q^2 , which is determined by the Fermi distribution in the correlation function $N_\sigma(\mathbf{q})$ (27). The QMC simulation for finite clusters show similar to Fig. 5, wave-vector dependence for the charge correlation function for the Hubbard model [see Fig. 4.5(a) in Ref. 17] and for the t - J model [see Fig. 3(b) in Ref. 18].

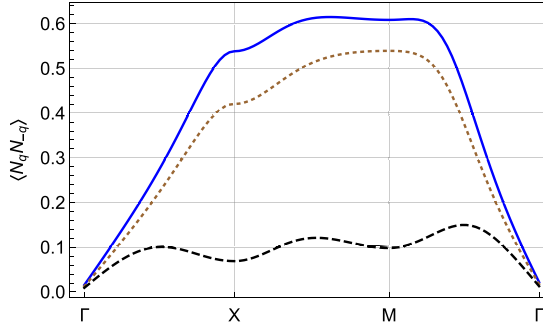


Fig. 5. (Color online) Correlation function $\langle N_q N_{-q} \rangle$ for $n = 0.7$ (blue, solid line), $n = 0.8$ (brown, dotted line), $n = 0.9$ (black, dash line).

3.2. Dynamical charge susceptibility

The spectral density of charge fluctuations (21) is calculated using the relations for the charge excitation energy $\Omega_{\mathbf{q}}$ (25) and the real and imaginary parts of the memory function (22) are given in the Appendix A, Eqs. (A.21), (A.23). At first, we consider the charge fluctuation damping $\Gamma(\mathbf{q}, \omega)$. Figures 6–8 show the energy dependence of the damping for several values of wave-vectors and electron concentrations $n = 0.9, 0.8, 0.7$. The damping tends to zero for $\omega \rightarrow 0$ and have a broad maximum at the energy of the order of $\Omega_{\mathbf{q}} \sim t$. Figure 9 demonstrates the damping at the charge excitation energy $\Gamma(\mathbf{q}, \omega = \Omega_{\mathbf{q}})$. The damping greatly increases at low hole concentrations as shown for $n = 0.9$, where electron correlations are strong and reveals maxima at $X(\pi, 0)$ and $M(\pi, \pi)$ points of the BZ. In that case, the damping $\Gamma(\mathbf{q}, \omega)$ becomes of the order of the charge excitation energy $\Omega_{\mathbf{q}}$ that results in a broad spectrum of the spectral density $I(\mathbf{q}, \omega)$ as shown in Figs. 10 and 11. At high-energy of the order of the charge excitation energy $\Omega_{\mathbf{q}} = 1 - 1.5$ at large hole doping, in particular at $n = 0.7$, the damping becomes weaker, $\Gamma(\mathbf{q}, \omega) \sim 0.5$, and a maximum in $I(\mathbf{q}, \omega)$ emerges at this energy as shown in Figs. 10 and 11. Similar

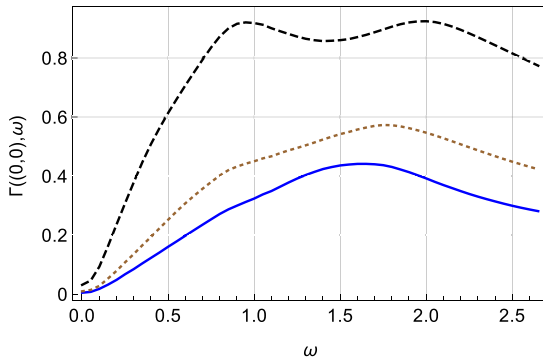


Fig. 6. (Color online) $\Gamma((0,0), \omega)$ at temperature $T = 0.02$ for $n = 0.7$ (blue, solid line), $n = 0.8$ (brown, dotted line), $n = 0.9$ (black, dash line).

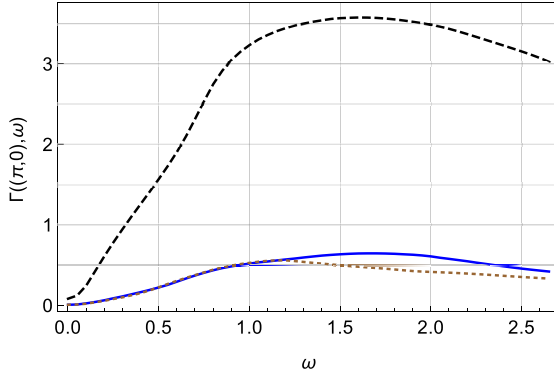


Fig. 7. (Color online) $\Gamma(\pi, 0, \omega)$ at temperature $T = 0.02$ for $n = 0.7$ (blue, solid line), $n = 0.8$ (brown, dotted line), $n = 0.9$ (black, dash line).

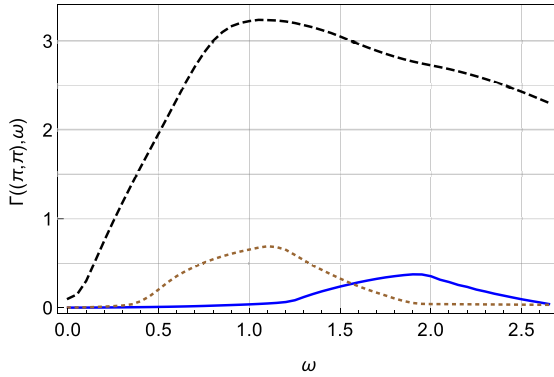


Fig. 8. (Color online) $\Gamma(\pi, \pi, \omega)$ at temperature $T = 0.02$ for $n = 0.7$ (blue, solid line), $n = 0.8$ (brown, dotted line), $n = 0.9$ (black, dash line).

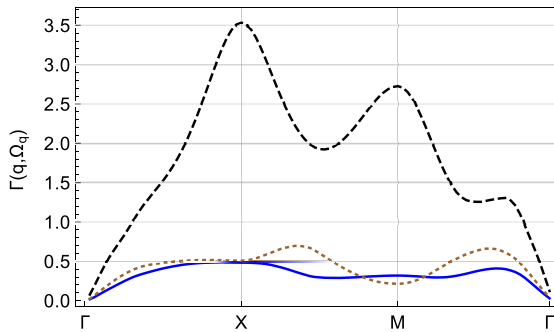


Fig. 9. (Color online) $\Gamma(\mathbf{q}, \Omega_{\mathbf{q}})$ along the main directions in the BZ: $\Gamma(0, 0) \rightarrow X(\pi, 0) \rightarrow M(\pi, \pi) \rightarrow \Gamma(0, 0)$ at temperature $T = 0.02$ for $n = 0.7$ (blue, solid line), $n = 0.8$ (brown, dotted line), $n = 0.9$ (black, dash line).

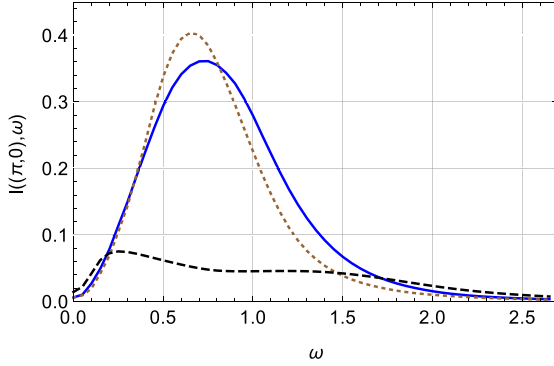


Fig. 10. (Color online) $I((\pi, 0), \omega)$ at temperature $T = 0.02$ for $n = 0.7$ (blue, solid line), $n = 0.8$ (brown, dotted line), $n = 0.9$ (black, dash line).

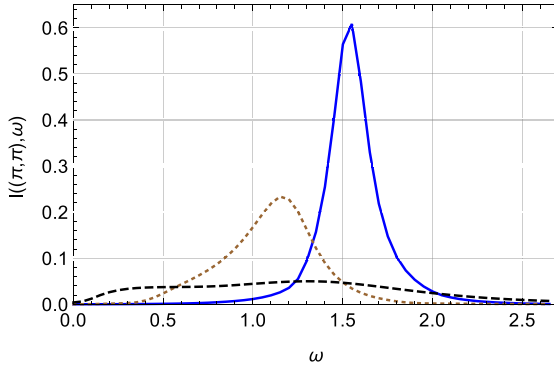


Fig. 11. (Color online) $I((\pi, \pi), \omega)$ at temperature $T = 0.02$ for $n = 0.7$ (blue, solid line), $n = 0.8$ (brown, dotted line), $n = 0.9$ (black, dash line).

maximum in charge fluctuations was found in the QMC simulation for the Hubbard model in Ref. 17 [see Fig. 4.2(b)].

The dispersions of low-energy charge excitations for $\omega = 0.05 \approx 20$ meV are shown in Figs. 12 and 13 along the directions $\Gamma(0, 0) \rightarrow M(\pi, \pi)$ and $\Gamma(0, 0) \rightarrow X(\pi, 0)$, respectively. We observe a maximum in excitations at small wave-vectors which are broad at low doping and sharper and more intensive at larger doping. The intensity of unidirectional excitations along $\Gamma(0, 0) \rightarrow X(\pi, 0)$ is higher in comparison with the diagonal direction $\Gamma(0, 0) \rightarrow M(\pi, \pi)$ due to weaker CI repulsion in the latter case, $V_3 < V_2$. In experiments for various cuprates, the charge density modulation is observed unidirectionally, along the Cu-O bonds which is explained by a stronger coupling along the bonds.

The intensity of the peaks increases for larger values of CI as demonstrated in Fig. 14. For higher temperatures, the damping increases which results in a more broad peak $I(\mathbf{q}, \omega)$ with lower intensity as shown in Fig. 15. The position of the peak in the spectral density (21) depends on the renormalization parameter, the real

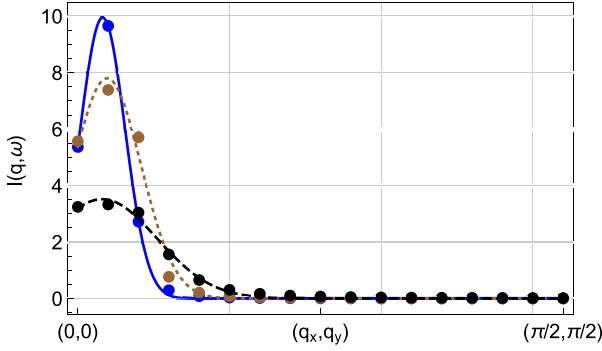


Fig. 12. (Color online) $I((q_x, q_y), \omega = 0.05)$ along the direction $\Gamma(0, 0) \rightarrow M(\pi, \pi)$ at temperature $T = 0.02$ for $n = 0.7$ (blue, solid line), $n = 0.8$ (brown, dotted line), $n = 0.9$ (black, dash line).

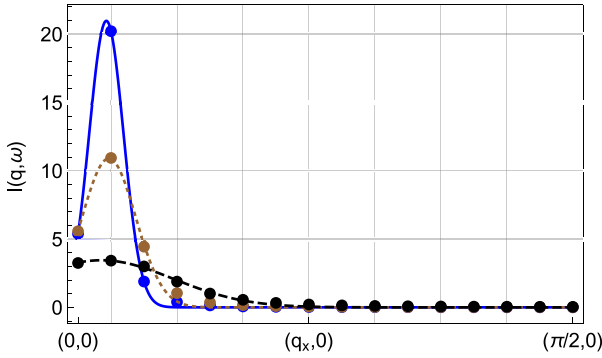


Fig. 13. (Color online) $I((q_x, q_y = 0), \omega = 0.05)$ along the direction $\Gamma(0, 0) \rightarrow X(\pi, 0)$ at temperature $T = 0.02$ for $n = 0.7$ (blue, solid line), $n = 0.8$ (brown, dotted line), $n = 0.9$ (black, dash line).

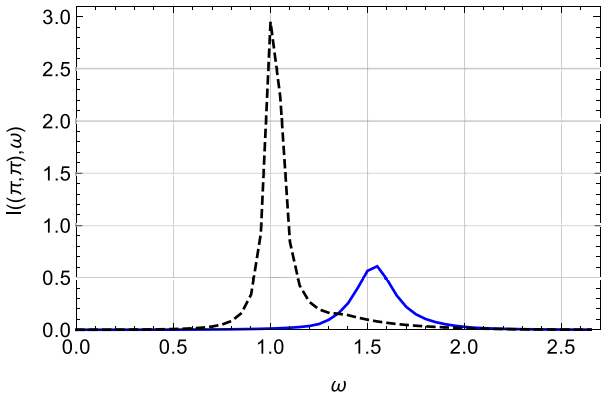


Fig. 14. (Color online) $I((\pi, \pi), \omega)$ at temperature $T = 0.02$ for $n = 0.7$ at $V_1 = 0.3$ (blue, solid line) and at $V_1 = 0.45$ (black, dash line).

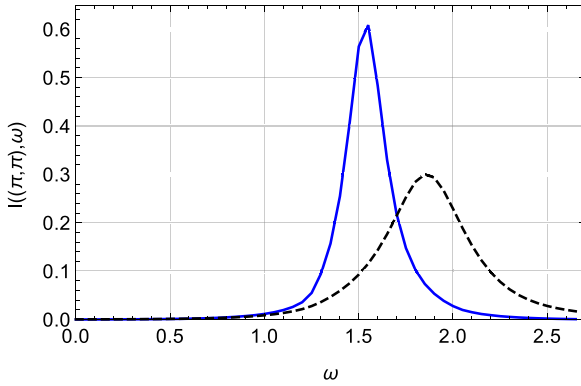


Fig. 15. (Color online) $I((\pi, \pi), \omega)$ for $n = 0.7$ depending on the temperature $T = 0.02$ (blue, solid line), $T = 0.05$ (black, dash line).

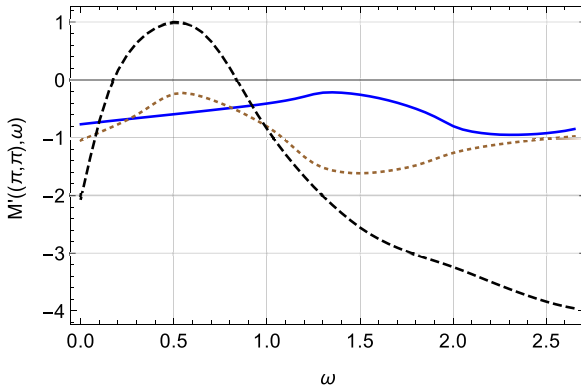


Fig. 16. (Color online) Real part of the self-energy $M'((\pi, \pi), \omega)$ at temperature $T = 0.02$ for $n = 0.7$ (blue, solid line), $n = 0.8$ (brown, dotted line), $n = 0.9$ (black, dash line).

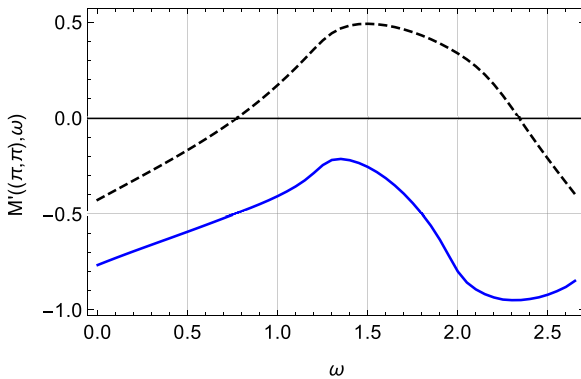


Fig. 17. (Color online) Real part of the self-energy $M'((\pi, \pi), \omega)$ for $n = 0.7$ depending on the temperature $T = 0.02$ (blue, solid line), $T = 0.05$ (black, dash line).

part of the memory function $M'(\mathbf{q}, \omega)$, which is quite large as shown in Fig. 16. The temperature dependence of $M'(\mathbf{q}, \omega)$ plotted in Fig. 17 for (π, π) -point of the BZ may change the position of the peak: for low-temperature $M'((\pi, \pi), \omega)$ is negative, while for larger temperature, $T = 0.5$, it becomes positive for energies close to the peak position at $\omega \sim 1.5$ which results in shifting the maximum of the peak to a higher-energy.

4. Conclusion

We have considered behavior of the static $\chi_{\mathbf{q}}$ and dynamic $\chi_{\mathbf{q}}(\omega)$ charge susceptibilities in a system of electrons with strong correlations in the framework of the t - J - V model at various hole doping. In several publications (see. e.g., Refs. 19–21) the DCS was calculated in the random-phase-type approximation using the representation for the density operator $N_{i\sigma} = X_i^{\sigma\sigma}$ as a product of single-particle Hubbard operators on the same unite site, $X_i^{\sigma\sigma} = X_i^{\sigma 0} X_i^{0\sigma}$, which is not unique in the Hubbard operator technique. In contrast to these works, we employ the original representation for the density operator (11) and have calculated the collective density–density GF. An exact representation for the DCS was derived within the projection method for the relaxation function. The memory function, both its real and imaginary parts, were calculated in the self-consistent Born approximation.

Studies of the static charge susceptibility have shown that for low hole concentrations it is small but strongly increases with doping. For a sufficiently strong intersite Coulomb repulsion, $\chi_{\mathbf{q}}$ diverges ($\chi_{\mathbf{q}}^{-1}$ vanishes) and CDWs arise in the system either along the diagonal of the unit cell (near the $M(\pi, \pi)$ -point of the BZ) or along the edge of the unit cell (near the $X(\pi, 0)$ -point of the BZ). The susceptibility weakly depends on other model parameters such as the anti-ferromagnetic exchange interaction J . Taking into account the damping of charge fluctuations described by the imaginary part of the memory function, we have found out that at low hole concentrations, e.g., for $\delta = 1 - n = 0.1$, due to strong correlations only a broad spectrum of overdamped charge fluctuations is observed. At large hole concentrations, the Fermi-like type behavior emerges and well-defined high-energy charge excitations appear close to $M(\pi, \pi)$ - and $X(\pi, 0)$ -points of the BZ. The dispersion of low-energy excitations demonstrates a maximum at small wave-vectors with the higher unidirectional intensity comparable with quasi-elastic excitations observed in experiments but with a weaker intensity at small doping contrary to experiments.

It should be pointed out that in the framework of the t - J - V model (1) derived for the Zhang-Rice singlets,³⁹ the inner structure of the unit cell of CuO_2 is not taken into account. Therefore, we cannot describe the d -wave CDWs detected in experiments at the oxygen sites or compare the obtained results quantitatively with experiments in cuprates. To study this problem, the more general p - d Emery model⁴⁰ should be considered where the matrix GF for p and d electron operators should be calculated which is beyond the scope of the present paper.

Appendix A. Memory Function

To calculate the relaxation function $\Phi_{\mathbf{q}}(\omega)$ (15), we use the projection method^{23,24} by composing the equations for the function $\Phi_{\mathbf{q}}(t - t')$ (13) after successively differentiating it with respect to two times, t and t' . In this case, we obtain a system of equations for the Fourier components of the relaxation functions as

$$\omega((N_{\mathbf{q}} | N_{-\mathbf{q}}))_{\omega} = \chi_{\mathbf{q}} + ((i\dot{N}_{\mathbf{q}} | N_{-\mathbf{q}}))_{\omega}, \quad (\text{A.1})$$

$$\omega((i\dot{N}_{\mathbf{q}} | N_{-\mathbf{q}}))_{\omega} = ((i\dot{N}_{\mathbf{q}} | -i\dot{N}_{-\mathbf{q}}))_{\omega}. \quad (\text{A.2})$$

The inhomogeneous term Eq. (A.1) is equal to $(N_{\mathbf{q}}, N_{-\mathbf{q}}) = \chi_{\mathbf{q}}$, while in Eq. (A.2), it is equal to zero, $(i\dot{N}_{\mathbf{q}}, N_{-\mathbf{q}}) = \langle [N_{\mathbf{q}}, N_{-\mathbf{q}}] \rangle = 0$. The solution of this set of equations can be written as

$$\Phi_{\mathbf{q}}(\omega) = \Phi_{\mathbf{q}}^0(\omega) + \Phi_{\mathbf{q}}^0(\omega)T_{\mathbf{q}}(\omega)\Phi_{\mathbf{q}}^0(\omega), \quad \Phi_{\mathbf{q}}^0(\omega) = \chi_{\mathbf{q}}/\omega, \quad (\text{A.3})$$

where we introduce the first-order scattering matrix as the current relaxation function $j_{\mathbf{q}} = \dot{N}_{\mathbf{q}} = -i[N_{\mathbf{q}}, H]$ as

$$T_{\mathbf{q}}(\omega) = (1/\chi_{\mathbf{q}}^2) ((j_{\mathbf{q}} | j_{-\mathbf{q}}))_{\omega}. \quad (\text{A.4})$$

To take only the irreducible part of the time dependence into account in the scattering matrix, we define the memory function of the first-order $M_{\mathbf{q}}^0(\omega) = ((j_{\mathbf{q}} | j_{-\mathbf{q}}))_{\omega}^{(\text{irr})}$ according to the equation

$$T_{\mathbf{q}}(\omega) = M_{\mathbf{q}}^0(\omega)/\chi_{\mathbf{q}}^2 + (M_{\mathbf{q}}^0(\omega)/\chi_{\mathbf{q}}^2) \Phi_{\mathbf{q}}^0(\omega)T_{\mathbf{q}}(\omega), \quad (\text{A.5})$$

which does not include the parts coupled by the “zero” relaxation function $\Phi_{\mathbf{q}}^0(\omega)$. Introducing the irreducible part of the time dependence for the current relaxation function is equivalent to the introduction of the projected Liouville operator for the time dependence of the correlation functions in the Mori method.²³ Using the function $M_{\mathbf{q}}^0(\omega)$, we can write the solution of Eq. (A.3) in the form

$$\Phi_{\mathbf{q}}(\omega) = \frac{\chi_{\mathbf{q}}}{\omega - M_{\mathbf{q}}^0(\omega)/\chi_{\mathbf{q}}}. \quad (\text{A.6})$$

For a consistent description of the charge density fluctuations, we must consider the second-order equation for the relaxation function by composing the equation for the memory function $M_{\mathbf{q}}^0(t - t')$ by differentiating it with respect to two times, t and t' . Introducing the memory function $M_{\mathbf{q}}(\omega)$ as the irreducible part of the scattering matrix in the equation for $M_{\mathbf{q}}^0(\omega)$ as in (A.3), we can write the corresponding solution as

$$M_{\mathbf{q}}^0(\omega) = \frac{m_{\mathbf{q}}}{\omega - M_{\mathbf{q}}(\omega)}. \quad (\text{A.7})$$

Here, the inhomogeneous term in the equation for $M_{\mathbf{q}}^0(t - t')$ becomes

$$m_{\mathbf{q}} = (i\dot{N}_{\mathbf{q}} | -i\dot{N}_{-\mathbf{q}}) = \langle [i\dot{N}_{\mathbf{q}}, N_{-\mathbf{q}}] \rangle, \quad (\text{A.8})$$

and the memory function $M_{\mathbf{q}}(\omega)$ is determined by the irreducible part of the “force” relaxation function $F_{\mathbf{q}} = (d/dt)j_{\mathbf{q}} = \ddot{N}_{\mathbf{q}}$ as

$$M_{\mathbf{q}}(\omega) = (1/m_{\mathbf{q}}) ((F_{\mathbf{q}} | F_{-\mathbf{q}}))_{\omega}^{(\text{irr})}. \quad (\text{A.9})$$

Taking relations (A.6) and (A.7) into account, we can write the relaxation function in the form given by Eq. (17):

$$\Phi_{\mathbf{q}}(\omega) = \chi_{\mathbf{q}} \frac{\omega - \omega M_{\mathbf{q}}(\omega)/m_{\mathbf{q}}}{\omega^2 - \Omega_{\mathbf{q}}^2 - \omega M_{\mathbf{q}}(\omega)/m_{\mathbf{q}}}. \quad (\text{A.10})$$

To complete the derivation of the relaxation function (A.10), we should calculate the correlation function $m_{\mathbf{q}}$ and the energy of charge density fluctuations $\Omega_{\mathbf{q}}^2$ in Eq. (23). The function $m_{\mathbf{q}}$ is defined by the first derivative of the density operator. Using the commutation relations of the HOs for the Hamiltonian (1), we obtain

$$i\dot{N}_i = [N_i, H] = - \sum_{j,\sigma} t_{ij} (X_i^{\sigma 0} X_j^{0\sigma} - X_j^{\sigma 0} X_i^{0\sigma}). \quad (\text{A.11})$$

Then for the correlation function, we have

$$m_{ij} = \langle [i\dot{N}_i, N_j] \rangle = 2\delta_{i,j} \sum_m t_{im} \langle X_i^{\sigma 0} X_m^{0\sigma} \rangle - 2t_{ij} \langle X_i^{\sigma 0} X_j^{0\sigma} \rangle + \text{H.c.} \quad (\text{A.12})$$

Using the Fourier transformation of m_{ij} , we get Eq. (24).

For calculation of the energy of charge density fluctuations $\Omega_{\mathbf{q}}^2$ in Eq. (23), we should consider the second derivative $-\ddot{N}_i$. Using the commutation relations of the HOs, we obtain

$$\begin{aligned} -\ddot{N}_i = [[N_i, H], H] &= \sum_{jm,\sigma\sigma'} t_{im} \left[(t_{mj} X_i^{\sigma 0} B_m^{\sigma'\sigma} X_j^{0\sigma'} - t_{ij} X_m^{\sigma 0} B_i^{\sigma'\sigma} X_j^{0\sigma'}) \right. \\ &\quad - \frac{1}{2} (J_{mj} X_i^{\sigma 0} X_m^{0\sigma'} - J_{ij} X_m^{\sigma 0} X_i^{0\sigma'}) (B_j^{\sigma'\sigma} - \delta_{\sigma,\sigma'}) \\ &\quad \left. - \delta_{\sigma,\sigma'} (V_{mj} - V_{ij}) N_j X_i^{\sigma 0} X_m^{0\sigma} \right] + \text{H.c.}, \end{aligned} \quad (\text{A.13})$$

where due to the completeness relation (8), we have

$$B_j^{\sigma'\sigma} = (X_j^{00} + X_j^{\sigma\sigma}) \delta_{\sigma'\sigma} + X_j^{\bar{\sigma}\sigma} \delta_{\sigma'\bar{\sigma}} = (1 - N_j/2 + \sigma S_j^z) \delta_{\sigma'\sigma} + S_j^{\bar{\sigma}} \delta_{\sigma'\bar{\sigma}}. \quad (\text{A.14})$$

The Fourier transformation of Eq. (A.13) results in the relation

$$\begin{aligned} -\ddot{N}_{\mathbf{q}} &= \frac{1}{N} \sum_{\sigma\sigma'} \sum_{\mathbf{k}, \mathbf{p}} [t(\mathbf{p}) - t(\mathbf{q} - \mathbf{p})] \left\{ \left[t(\mathbf{k}) - \frac{1}{2} J(\mathbf{k} + \mathbf{p}) \right] X_{\mathbf{q}-\mathbf{p}}^{\sigma 0} X_{\mathbf{k}}^{0\sigma'} B_{\mathbf{k}+\mathbf{p}}^{\sigma'\sigma} \right. \\ &\quad \left. + \delta_{\sigma\sigma'} V(\mathbf{k} + \mathbf{p}) X_{\mathbf{q}-\mathbf{p}}^{\sigma 0} X_{\mathbf{k}}^{0\sigma} N_{\mathbf{k}+\mathbf{p}} \right\} + \text{H.c.} \end{aligned} \quad (\text{A.15})$$

Now, we consider the scalar product $(-\ddot{N}_{\mathbf{q}}, N_{-\mathbf{q}})$. The second derivative $-\ddot{N}_i$ (A.13) in the direct space reveals that it depends on products of three fermionic- and

bosonic-type operators which refer to different lattice sites and therefore their correlation function, can be decoupled into independent correlation functions. For instance, we can write

$$\begin{aligned} \langle X_{\mathbf{q}-\mathbf{p}}^{\sigma 0} B_{\mathbf{k}+\mathbf{p}}^{\sigma' \sigma} X_{\mathbf{k}}^{0 \sigma'}, N_{-\mathbf{q}} \rangle &= \langle X_{\mathbf{q}-\mathbf{p}}^{\sigma 0} X_{\mathbf{k}}^{0 \sigma'} \rangle \langle B_{\mathbf{k}+\mathbf{p}}^{\sigma' \sigma}, N_{-\mathbf{q}} \rangle \\ &= -(1/2) \delta_{\mathbf{q}-\mathbf{p}, \mathbf{k}} \delta_{\sigma' \sigma} \langle X_{\mathbf{k}}^{\sigma 0} X_{\mathbf{k}}^{0 \sigma} \rangle (N_{\mathbf{q}}, N_{-\mathbf{q}}), \end{aligned} \quad (\text{A.16})$$

where only the number operator N_i in $B_j^{\sigma' \sigma}$ in (A.14) gives a contribution to the scalar product. Using this approximation, we obtain for the spectrum of charge fluctuation Eq. (25).

Now, we calculate the memory function (19) in the DCS (20) which is defined by the equation $M_{\mathbf{q}}(\omega) = ((F_{\mathbf{q}} | F_{-\mathbf{q}}))_{\omega}^{\text{irr}} = ((\ddot{N}_{\mathbf{q}} | \ddot{N}_{-\mathbf{q}}))_{\omega}^{\text{irr}}$. Using the spectral representation for the retarded GFs,²⁵ the memory function can be written as the many-particle time-dependent correlation function

$$M_{\mathbf{q}}(\omega) = \frac{1}{2\pi} \int_{-\infty}^{\infty} d\omega' \frac{e^{\beta\omega'} - 1}{\omega'(\omega - \omega')} \int_{-\infty}^{\infty} dt e^{i\omega't} \langle \ddot{N}_{-\mathbf{q}} \ddot{N}_{\mathbf{q}}(t) \rangle^{\text{irr}}. \quad (\text{A.17})$$

Assuming an independent propagation of electronic and charge excitations on different lattice sites given in Eq. (A.13), we can decouple the many-particle time-dependent correlation functions into products of single-particle time-dependent correlation functions similar to the decoupling in Eq. (A.16) above. For instance, taking into account that $N_{-\mathbf{q}} = N_{\mathbf{q}}^{\dagger}$ for the charge fluctuation contribution, we obtain

$$\begin{aligned} \langle X_{\mathbf{q}-\mathbf{p}}^{0 \sigma} X_{\mathbf{k}}^{\sigma 0} N_{\mathbf{k}+\mathbf{p}}^{\dagger} X_{\mathbf{q}'-\mathbf{p}'}^{\sigma' 0}(t) X_{\mathbf{k}'}^{0 \sigma'}(t) N_{\mathbf{k}'+\mathbf{p}'}(t) \rangle \\ = \delta_{\sigma, \sigma'} \delta_{\mathbf{k}, \mathbf{k}'} \delta_{\mathbf{p}, \mathbf{p}'} \langle X_{\mathbf{q}-\mathbf{p}}^{0 \sigma} X_{\mathbf{q}-\mathbf{p}}^{\sigma 0}(t) \rangle \langle X_{\mathbf{k}}^{\sigma 0} X_{\mathbf{k}}^{0 \sigma}(t) \rangle \langle N_{\mathbf{k}+\mathbf{p}}^{\dagger} N_{\mathbf{k}+\mathbf{p}}(t) \rangle. \end{aligned} \quad (\text{A.18})$$

The time-dependent correlation functions in Eq. (A.18), can be calculated from the spectral representations²⁵

$$\langle BA(t) \rangle = \int_{-\infty}^{\infty} d\omega e^{-i\omega t} f(\omega) [-(1/\pi)] \text{Im} \langle \langle A | B \rangle \rangle_{\omega}, \quad (\text{A.19})$$

where $f(\omega)$ is the Fermi function $n(\omega)$ for the correlation function $\langle X_{\mathbf{k}}^{\sigma 0} X_{\mathbf{k}}^{0 \sigma}(t) \rangle$ and the Bose function $N(\omega)$ for the charge correlation functions. Considering the lowest order approximation for the single-particle correlation functions in Eq. (A.18), we use the MFA for the corresponding GFs:

$$\begin{aligned} A_{\mathbf{k}}(\omega) &= -\frac{1}{\pi} \text{Im} \langle \langle X_{\mathbf{k}}^{0 \sigma} | X_{\mathbf{k}}^{\sigma 0} \rangle \rangle_{\omega+i\delta} = Q \delta(\omega - \tilde{\epsilon}_{\mathbf{k}}), \\ -\frac{1}{\pi} \text{Im} \langle \langle N_{\mathbf{p}} | N_{\mathbf{p}}^{\dagger} \rangle \rangle_{\omega+i\delta} &= \frac{1}{2\Omega_{\mathbf{p}}} [\delta(\omega - \Omega_{\mathbf{p}}) - \delta(\omega + \Omega_{\mathbf{p}})]. \end{aligned} \quad (\text{A.20})$$

Integration over time t in Eq. (A.17) results in final formula for $M_{\mathbf{q}}(\omega)$ (A.9).

In particular, for the damping of charge fluctuations (22) $\Gamma_{\mathbf{q}}(\omega)$ which is determined by the imaginary part of the memory function $M_{\mathbf{q}}''(\omega) = \text{Im} M_{\mathbf{q}}(\omega + i\varepsilon)$,

we obtain

$$\begin{aligned}
 \Gamma(\mathbf{q}, \omega) = & \frac{\exp(\beta\omega) - 1}{m_{\mathbf{q}}\omega} \frac{Q^2}{N^2} \sum_{\mathbf{p}, \mathbf{k}} \left[\frac{1}{4} (A(\mathbf{q}, \mathbf{k}, \mathbf{p})^2 + B(\mathbf{q}, \mathbf{k}, \mathbf{p})^2) + C(\mathbf{q}, \mathbf{k}, \mathbf{p})^2 \right] \\
 & \times \frac{1}{\Omega_{\mathbf{p}}} \{ n(\tilde{\varepsilon}_{\mathbf{k}}) [1 - n(\tilde{\varepsilon}_{\mathbf{k}-\mathbf{p}+\mathbf{q}})] (N(\Omega_{\mathbf{p}}) \delta(\omega - \tilde{\varepsilon}_{\mathbf{k}} + \tilde{\varepsilon}_{\mathbf{k}-\mathbf{p}+\mathbf{q}} - \Omega_{\mathbf{p}})) \\
 & + [1 + N(\Omega_{\mathbf{p}})] \delta(\omega - \tilde{\varepsilon}_{\mathbf{k}} + \tilde{\varepsilon}_{\mathbf{k}-\mathbf{p}+\mathbf{q}} + \Omega_{\mathbf{p}})) \\
 & + [1 - n(\tilde{\varepsilon}_{\mathbf{k}})] n(\tilde{\varepsilon}_{\mathbf{k}-\mathbf{p}+\mathbf{q}}) (N(\Omega_{\mathbf{p}}) \delta(\omega + \tilde{\varepsilon}_{\mathbf{k}} - \tilde{\varepsilon}_{\mathbf{k}-\mathbf{p}+\mathbf{q}} - \Omega_{\mathbf{p}})) \\
 & + [1 + N(\Omega_{\mathbf{p}})] \delta(\omega + \tilde{\varepsilon}_{\mathbf{k}} - \tilde{\varepsilon}_{\mathbf{k}-\mathbf{p}+\mathbf{q}} + \Omega_{\mathbf{p}})) \}. \tag{A.21}
 \end{aligned}$$

Here, the interaction functions are given by

$$\begin{aligned}
 A(\mathbf{q}, \mathbf{k}, \mathbf{p}) &= [t(\mathbf{k} - \mathbf{p}) - t(\mathbf{k} - \mathbf{p} + \mathbf{q})] t(\mathbf{k}), \\
 B(\mathbf{q}, \mathbf{k}, \mathbf{p}) &= [t(\mathbf{k} - \mathbf{p}) - t(\mathbf{k} - \mathbf{p} + \mathbf{q})] J(\mathbf{p}), \\
 C(\mathbf{q}, \mathbf{k}, \mathbf{p}) &= [t(\mathbf{k} - \mathbf{p} + \mathbf{q}) - t(\mathbf{k} - \mathbf{p})] V(\mathbf{p}).
 \end{aligned} \tag{A.22}$$

The real part of the memory function $M'_{\mathbf{q}}(\omega) = \text{Re}M_{\mathbf{q}}(\omega + i\varepsilon)$ is calculated from the dispersion relation

$$M'(\omega) = \frac{1}{\pi} \int_{-\infty}^{\infty} d\omega' \frac{M''(\omega')}{\omega' - \omega}. \tag{A.23}$$

It is important to point out that in the equation of motion method for the GF for the memory function and the damping of charge fluctuations (22), we have found out that these functions are described by the decay process of charge fluctuations into a particle-hole pair accompanied by a bosonic excitation. In the commonly used RPA, the decay process is described only by a creation of particle-hole pairs which results in quite different kinematics given by the conservation laws for momenta and energies.

Appendix B. Electronic Spectrum

To calculate the electronic spectrum in the extended t - J - V model (1) with the intersite CI, we use the results of Ref. 34. From the equations of motion for the single-particle GF²⁵

$$G_{ij,\sigma}(t - t') = \langle\langle X_i^{0\sigma}(t) | X_j^{\sigma 0}(t') \rangle\rangle, \tag{B.1}$$

we obtain the zero-order GF in the generalized MFA

$$G_{ij\sigma}^0(\omega) = Q \{ \omega \delta_{ij} - \varepsilon_{ij\sigma} \}^{-1}, \tag{B.2}$$

where the frequency matrix

$$\begin{aligned}
 \varepsilon_{ij\sigma} &= \langle\langle [X_i^{0\sigma}, H], X_j^{\sigma 0} \rangle\rangle Q^{-1}, \\
 Q &= \langle X_i^{00} + X_i^{\sigma\sigma} \rangle = 1 - n/2.
 \end{aligned} \tag{B.3}$$

In \mathbf{q} -representation, the GF (B.2) and the renormalized spectrum of electronic excitations are given by

$$G^0(\mathbf{q}, \omega) = Q \frac{1}{\omega - \tilde{\varepsilon}(\mathbf{q})}, \quad (\text{B.4})$$

$$\tilde{\varepsilon}(\mathbf{q}) = -4t \alpha \gamma(\mathbf{q}) - 4t' \beta \gamma'(\mathbf{q}) - 4t'' \beta \gamma''(\mathbf{q}) + \omega^{(c)}(\mathbf{q}) - \mu, \quad (\text{B.5})$$

$$\omega^{(c)}(\mathbf{q}) = \frac{1}{N} \sum_{\mathbf{k}} V(\mathbf{q} - \mathbf{k}) N(\mathbf{k}). \quad (\text{B.6})$$

The renormalization of the spectrum (B.5) caused by the AF short-range order is determined by the parameters

$$\alpha = Q \left[1 + \frac{C_1}{Q^2} \right], \quad \beta = Q \left[1 + \frac{C_2}{Q^2} \right], \quad (\text{B.7})$$

where the spin correlation functions for the first and the next neighbors are

$$C_1 = \langle \mathbf{S}_i \mathbf{S}_{i \pm a_x / a_y} \rangle = \frac{1}{N} \sum_{\mathbf{q}} \gamma(\mathbf{q}) C_{\mathbf{q}},$$

$$C_2 = \langle \mathbf{S}_i \mathbf{S}_{i \pm a_x \pm a_y} \rangle = \frac{1}{N} \sum_{\mathbf{q}} \gamma'(\mathbf{q}) C_{\mathbf{q}}. \quad (\text{B.8})$$

For the spin correlation function $C_{\mathbf{q}} = \langle \mathbf{S}_{\mathbf{q}} \mathbf{S}_{-\mathbf{q}} \rangle$, we take the model³⁴

$$C_{\mathbf{q}} = \frac{C_{\mathbf{Q}}}{1 + \xi^2 [1 + \gamma(\mathbf{q})]}, \quad C_{\mathbf{Q}} = \frac{3n}{4} \left\{ \frac{1}{N} \sum_{\mathbf{q}} \frac{1}{1 + \xi^2 [1 + \gamma(\mathbf{q})]} \right\}^{-1}, \quad (\text{B.9})$$

where the parameter $C_{\mathbf{Q}}$ is defined from the normalization condition $\langle \mathbf{S}_i \mathbf{S}_i \rangle = (3/4)n = (1/N) \sum_{\mathbf{q}} C_{\mathbf{q}}$. The spin correlation function $C_{\mathbf{q}}$ is determined by the AF correlation length ξ and has the maximum at the AF wave-vector $\mathbf{Q} = (\pi, \pi)$, where $\gamma(\mathbf{Q}) = -1$. The values of correlation functions C_1, C_2 , the AF correlation length ξ , and parameters α, β for various hole doping δ are given in Table B.1. The contribution $\omega^{(c)}$ (B.6) from the CI for parameters $V_1 = 0.3, V_2 = 0.2$ appears to be small, of the order of few percents, and is ignored in the calculations.

For the hopping parameters $t' = 0.1t, t'' = 0.2t$, we obtain the electronic spectrum shown in Fig. B.1, which is similar to that calculated within the Hubbard

Table B.1. Static spin correlation functions C_1, C_2 , AF correlation length ξ , and the renormalization parameters (B.7) at various hole concentrations $\delta = 1 - n$.

$\delta =$	0.05	0.10	0.20	0.30
C_1	-0.26	-0.21	-0.14	-0.10
C_2	0.16	0.11	0.06	0.04
ξ	3.40	2.50	1.70	1.40
α	0.03	0.17	0.37	0.50
β	0.83	0.75	0.72	0.71

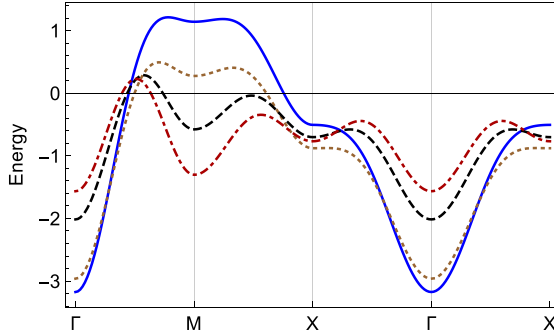


Fig. B.1. (Color online) Dispersion of the electron spectrum along the main directions in the BZ: $\Gamma(0,0) \rightarrow X(\pi,0) \rightarrow M(\pi,\pi) \rightarrow \Gamma(0,0)$ for $n = 0.7$ (blue, solid line), $n = 0.8$ (brown, dotted line), $n = 0.9$ (black, dash line), $n = 0.95$ (red, dash-dotted line).

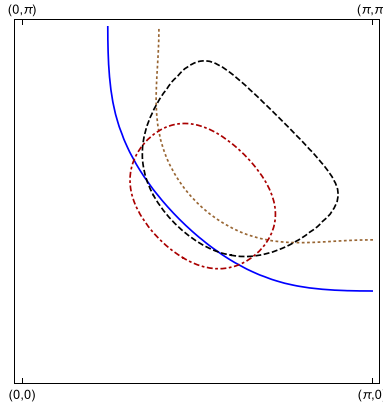


Fig. B.2. (Color online) Fermi surface in the quarter of the BZ for $n = 0.7$ (blue, solid line), $n = 0.8$ (brown, dotted line), $n = 0.9$ (black, dash line), $n = 0.95$ (red, dash-dotted line).

model in Ref. 37 (for details see Ref. 36). Namely, the renormalization of the spectrum induced by the spin correlation functions (B.8) provides the FS $\tilde{\epsilon}_{\mathbf{k}_F} = 0$ with hole pockets at low doping as shown in Fig. B.2. Note that emerging of the hole pockets results in the pseudogap state with a low density of states in the region close to $(\pm\pi, 0)$, $(0, \pm\pi)$ points in the BZ.

References

1. N. M. Plakida, *High-Temperature Cuprate Superconductors*, Springer Series in Solid-State Sciences, Vol. 166 (Springer-Verlag, Berlin, 2010).
2. S. Blanco-Canosa *et al.*, *Phys. Rev. B* **90**, 054513 (2014).
3. M. Hücker *et al.*, *Phys. Rev. B* **90**, 054514 (2014).
4. R. Comin *et al.*, *Nature Mater.* **14**, 796 (2015).
5. R. Comin *et al.*, *Science* **347**, 1335 (2015).
6. R. Comin *et al.*, *Science* **343**, 390 (2014).
7. M. Hashimoto *et al.*, *Phys. Rev. B* **89**, 220511(R) (2014).

8. E. H. da Silva Neto *et al.*, *Science* **343**, 393 (2014).
9. M. H. Hamidian *et al.*, *Nat. Phys.* **12**, 150 (2016).
10. Y. Y. Peng *et al.*, *Phys. Rev. B* **94**, 184511 (2016).
11. W. Tabis *et al.*, *Nature Commun.* **5**, 5875 (2014).
12. G. Campi *et al.*, *Nature* **25**, 359 (2015).
13. Yu. Wang and A. V. Chubukov, *Phys. Rev. B* **92**, 245140 (2015).
14. S. Caprara *et al.*, *Phys. Rev. B* **95**, 224511 (2017).
15. P. A. Volkov and K. B. Efetov, *Phys. Rev. B* **93**, 085131 (2016).
16. J. Hubbard, *Proc. Roy. Soc. A (London)* **285**, 542 (1965).
17. E. Bulut, *Adv. Phys.* **51**, 1587 (2002).
18. Y. C. Chen *et al.*, *Phys. Rev. B* **50**, 655(R) (1994).
19. I. Eremin *et al.*, *Phys. Rev. B* **56**, 11305 (1997).
20. M. Eremin, S. Varlamov and I. Eremin, *Appl. Magn. Reson.* **19**, 355 (2000).
21. M. Eremin, I. Eremin and S. Varlamov, *Phys. Rev. B* **64**, 214512 (2001).
22. M. V. Eremin and M. A. Malakhov, *JETP Lett.* **100**, 324 (2014).
23. H. Mori, *Prog. Theor. Phys.* **34**, 399 (1965).
24. N. M. Plakida, in *Theoretical Methods for Strongly Correlated Systems*, eds. A. Avella and F. Mancini, Springer Series in Solid-State Sciences, Vol. 171, Chap. 6 (Springer, Heidelberg, 2011), pp. 173–202.
25. D. N. Zubarev, *Sov. Phys. Usp.* **3**, 320 (1960); *Nonequilibrium Statical Thermodynamics* (Consultant Bureau, New-York, 1974).
26. A. A. Vladimirov, D. Ihle and N. M. Plakida, *Phys. Rev. B* **80**, 104425 (2009).
27. A. A. Vladimirov, D. Ihle and N. M. Plakida, *Phys. Rev. B* **83**, 024411 (2011).
28. A. A. Vladimirov, D. Ihle and N. M. Plakida, *Phys. Rev. B* **85**, 224536 (2012).
29. W. Götze and P. Wölfle, *Phys. Rev. B* **6**, 1226 (1972).
30. D. Forster, *Hydrodynamic Fluctuations, Broken Symmetry and Correlation Functions* (Benjamin, New York, 1975).
31. Yu. A. Tserkovnikov, *Theor. Math. Fiz.* **50**, 261 (1982).
32. G. Jackeli and N. M. Plakida, *Phys. Rev. B* **60**, 5266 (1999).
33. N. D. Tung and N. M. Plakida, *Theor. Math. Phys.* **194**, 126 (2018).
34. N. M. Plakida and V. S. Oudovenko, *Phys. Rev. B* **59**, 11949 (1999).
35. Yu. A. Izyumov and Yu. N. Scryabin, *Statistical Mechanics of Magnetically Ordered Systems* (Consultant Bureau, New York, 1989).
36. N. M. Plakida and V. S. Oudovenko, *J. Exp. Theor. Phys.* **104**, 230 (2007).
37. N. M. Plakida and V. S. Oudovenko, *Eur. Phys. J. B* **86**, 115 (2013).
38. L. F. Feiner, J. H. Jefferson and R. Raimondi, *Phys. Rev. B* **53**, 8751 (1996).
39. F. C. Zhang and T. M. Rice, *Phys. Rev. B* **37**, 3759 (1988).
40. V. Emery, *Phys. Rev. Lett.* **58**, 2794 (1987).